Minimum Energy Consumption in Multicomponent Distillation. 1. V_{min} Diagram for a Two-Product Column

Ivar J. Halvorsen† and Sigurd Skogestad*

Department of Chemical Engineering, Norwegian University of Science and Technology, N-7491 Trondheim, Norway

The V_{min} diagram is introduced to effectively visualize how the minimum energy consumption is related to the feed-component distribution for all possible operating points in a two-product distillation column with a multicomponent feed. The classical Underwood equations are used to derive analytical expressions for the ideal case with constant relative volatility and constant molar flows. However, the diagram can also be used for nonideal mixtures. The V_{min} diagram is very insightful for assessing multicomponent separation in a single column and is even more powerful for complex column arrangements, such as Petlyuk columns (parts 2 and 3 of this series of papers).

1. Introduction

We assume constant molar flows, constant relative volatilities, and an infinite number of stages and use the classical Underwood equations to compute the distribution of all of the components in the generalized multicomponent feed as a function of the degrees of freedom in a two-product distillation column (Figure 1).

The main result is the simple graphical visualization of minimum energy as a function of the feed distribution. We denote this as the minimum-energy mountain diagram or just the V_{min} diagram.

The V_{min} diagram can be used for quick determination of the minimum energy requirement in a single binary column with a multicomponent feed, for any feasible product specification.

The equations of Underwood[1−4] have been applied successfully by many authors for the analysis of multicomponent distillation, e.g., Shiras et al.,[5] King,[6] Franklin and Forsyth,[7] and Wachter et al.,[8] and in a comprehensive review of minimum-energy calculations by Koehler et al.[9] Minimum-energy expressions for Petlyuk arrangements with three components have been presented by Fidkowski and Krolikowski[10] and Carlberg and Westerberg.[11,12] However, minimum energy requirements for the general multicomponent case, the topic of this paper, have so far not been well understood.

Alternative methods for visualization of feed distribution regions for a single column have been presented by Wachter et al.[8] based on a continuum model and by Neri et al.[13] based on equilibrium theory.

Our original derivation of the V_{min} diagram was based on computing pinch zone compositions for columns with an infinite number of stages. However, the Underwood approach is simpler and may easily be extended to other kinds of column section interconnections. Specifically, the methods presented can also be used for Petlyuk arrangements and for arrangements with side strippers and side rectifiers. This is treated in detail in the thesis by Halvorsen[14] and in the succeeding papers on minimum-energy consumption in distillation, parts 2[15] and 3[16] of this series. The behavior of composition profiles and pinch zones in a column and how the required finite number of stages depends on the component distribution are also treated in more detail in the thesis.[14]

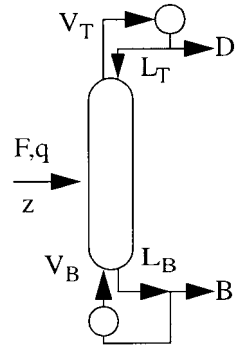

Figure 1. Two-product distillation column with a reboiler and total condenser.

We may alternatively compute V_{min} diagrams by other means, e.g., by a few simulations for a real system with a rigorous simulator. Thus, the insight provided by the V_{min} diagram is not limited to ideal systems. However, with the Underwood equations and the ideal system assumption, we are able to deduce exact analytical expressions for minimum-energy calculations.

2. Problem Definition: Degrees of Freedom

With a given feed, a two-product distillation column normally has 2 steady-state degrees of freedom of operation. For a binary feed, this is sufficient to specify any product distribution. In the case of a multicomponent feed, however, we cannot freely specify the compositions in both products. In practice, one usually specifies the distribution of two key components, and the distribution of the nonkey components is then completely determined for a given feed. In some cases, the column pressure could be considered as a third degree of freedom, but we will assume that the pressure is constant throughout this paper because the pressure has a limited impact on the product distribution.

* To whom correspondence should be addressed. Phone: +47 73594030. Fax: +47 73594080. E-mail: Sigurd.Skogestad@chemeng.ntnu.no.

† Current address: SINTEF Electronics and Cybernetics, N-7465 Trondheim, Norway. E-mail: Ivar.J.Halvorsen@sintef.no.

10.1021/ie010863g CCC: $25.00
Published on Web 01/01/2003

For every possible operating point, we want to find the normalized vapor flow rate (V/F), the overall product split (D/F or B/F), and the distribution, here given by the set of recoveries $R = [r_1, r_2, ..., r_{N_c}]$. This can be expressed for the top section as

$$\left[\frac{V_T}{F}, \frac{D}{F}, R_T\right] = f(\text{Spec}_1, \text{Spec}_2, \text{feed properties}) \quad (1)$$

It is sufficient to consider only one of the top or bottom sections because the recoveries and flows in the other section can be found by a material balance at the feed stage. The feed properties are given by the composition vector **z**, flow rate F, liquid fraction q, and relative volatilities α. The recovery (r_i) is the amount of component i transported in a stream or through a section divided by the amount in the feed. N_c is the number of components.

3. Underwood Equations for Minimum Energy

3.1. Some Basic Definitions. The starting point for Underwood's methods for multicomponent mixtures[1−4] is the material balance equation at a cross section in the column. The net material transport (w_i) of component i upward through a stage n is the difference between the amount travelling upward from a stage as vapor and the amount entering a stage from above as liquid:

$$w_i = V_n y_{i,n} - L_{n+1} x_{i,n+1} \quad (2)$$

Note that at steady state w_i is constant through each column section. In the following, we assume constant molar flows ($L = L_n = L_{n-1}$ and $V = V_n = V_{n+1}$) and constant relative volatility (α_i).

The vapor−liquid equilibrium (VLE) at an equilibrium stage is given by

$$y_i = \frac{\alpha_i x_i}{\sum_{i=1}^{N_c} \alpha_i x_i} \quad (3)$$

In the top section, the net product flow is $D = V_n - L_{n+1}$ and

$$w_{i,T} = x_{i,D} D = r_{i,D} z_i F \quad (4)$$

In the bottom section, $B = L_{n+1} - V_n$, and the net material flow is

$$w_{i,B} = -x_{i,B} B = r_{i,B} z_i F \quad (5)$$

The positive direction of the net component flows is defined upward, but in the bottom the components normally travel downward from the feed stage and then we have $w_{i,B} \leq 0$. With a single feed stream, the net component flow in the feed is given as

$$w_{i,F} = z_i F \quad (6)$$

A recovery can then be regarded as a normalized component flow:

$$r_i = w_i / w_{i,F} = w_i / z_i F \quad (7)$$

At the feed stage, $w_{i,F}$ is defined as positive into the column. Note that with our definition in (7) the recovery is also a signed variable.

3.2. Definition of Underwood Roots. The Underwood roots (ϕ) in the top section are defined as the N_c solutions of

$$V_T = \sum_{i=1}^{N_c} \frac{\alpha_i w_{i,T}}{\alpha_i - \phi} \quad (8)$$

In the bottom there is another set of Underwood roots ψ given by the solutions of

$$V_B = \sum_{i=1}^{N_c} \frac{\alpha_i w_{i,B}}{\alpha_i - \psi} \quad (9)$$

Note that these equations are related via the material balance at the feed stage:

$$w_{i,T} - w_{i,B} = w_{i,F} = z_{i,F} F \quad (10)$$

(which is equivalent to $r_{i,T} - r_{i,B} = 1$) and the change in vapor flow at the feed stage given by the liquid fraction (q) of the feed (F)

$$V_F = V_T - V_B = (1 - q)F \quad (11)$$

Computation of the Underwood roots involves solving a straightforward polynomial root problem, but we should be careful and make sure that the vector of component flows w_T or w_B is feasible. This also implies that in the multicomponent case there is a "hidden" interaction between the unspecified elements in w_T and the Underwood roots.

3.3. Underwood Roots for Minimum Vapor Flow. Underwood showed a series of properties of the roots (ϕ and ψ) for a two-product column with a single reboiler and condenser. In this conventional column, all components flow upward in the top section ($w_{i,T} \geq 0$) and downward in the bottom section ($w_{i,B} \leq 0$). With N_c components there are, for each of ϕ and ψ, N_c solutions obeying

$$\alpha_1 > \phi_1 > \alpha_2 > \phi_2 > \alpha_3 > ... > \alpha_{N_c} > \phi_{N_c} \quad (12)$$

$$\psi_1 > \alpha_1 > \psi_2 > \alpha_2 > \psi_3 > \alpha_3 > ... > \psi_{N_c} > \alpha_{N_c} \quad (13)$$

When the vapor flow is reduced, the roots in the top section will decrease, while the roots in the bottom section will increase. Underwood[2] showed that, at minimum vapor flow for any given product distribution, one or more pairs of roots coincide to a common root (denoted θ_i, i.e., $\phi_i = \psi_{i+1} = \theta_i$).

Recall that $V_T - V_B = (1 - q)F$. By subtracting the defining equations for the top and bottom sections (8) and (9), we obtain the following equation, which is valid for the common roots only (denoted θ):

$$1 - q = \sum_i \frac{\alpha_i z_i}{\alpha_i - \theta} \quad (14)$$

We call this expression the *feed equation* because only the feed properties (q and z) appear. It has also N_c roots, but one of these cannot be a common root due to (12) and (13), so there are $N_c - 1$ possible common roots that

Table 1. Number of Unknown Variables and Equations

	total number of variables (V_T, R_T)	$N_c + 1$
−	no. of nondistributing components	$N_c - N_d$
	remaining unknown variables	$N_d + 1$
−	no. of equations = no. of active roots N_a	$N_d - 1$
	degrees of freedom	2

obey

$$\alpha_1 > \theta_1 > \alpha_2 > \theta_2 > \ldots > \theta_{N_c-1} > \alpha_{N_c} \qquad (15)$$

We will denote a root θ_k an *active* root for the case when $\phi_k = \psi_{k+1} = \theta_k$. Inserting the active root in the top- and bottom-defining equations gives the minimum flow for a given set of component distributions (w_T or r_T).

$$V_{T,\min} = \sum_i \frac{\alpha_i w_{i,T}}{\alpha_i - \theta_k} \quad \text{or} \quad V_{T,\min} = \sum_i \frac{\alpha_i r_{i,T} z_i F}{\alpha_i - \theta_k} \qquad (16)$$

With N_a active roots, this represents a set of N_a independent linear equations, which may be used to find the exact set of the so-called *distributing* components that appear in both products.

Note that the subscript min indicates minimum vapor flow, and then we use a common root θ from (14) as opposed to an actual root ϕ in (8).

3.4. Computational Procedure. Our task is to find the N_c product recoveries (or component flows) and the vapor flow, given any pair of feasible specifications. The procedure on how to apply Underwood's equations for this purpose has been described by several authors, e.g., Shiras[5] and Carlberg and Westerberg.[11]

The key to the general solution is to identify the *distributing* components. A component in the feed is distributing if it appears in both products or is exactly at the limit of becoming distributing if the vapor flow is reduced with an infinitesimal amount.

The computation procedure is as follows:

Consider a set of N_d distributing components, denoted as $\{d_1, d_2, \ldots, d_{N_d}\}$. The recoveries in the top are trivially $r_{i,T} = 1$ for all nondistributing light components ($i < d_1$) and $r_{i,T} = 0$ for the nondistributing heavy components ($i > d_{N_d}$). Then, with a given distribution set, we know the $N_c - N_d$ recoveries of the nondistributing components.

Then use another of Underwood's results: For any minimum vapor flow solution, the active Underwood roots will only be those with values in the range between the volatilities of the distributing components ($\alpha_{d_1} > \theta_k > \theta_{d_{Nd}}$). This implies that, with N_d distributing components, the number of active roots is

$$N_a = N_d - 1 \qquad (17)$$

Thus, from Table 1, we see that by making two specifications we have enough information to determine the solution completely.

Define the vector $\mathbf{X}$ containing the recoveries of the N_d distributing components and the normalized vapor flow in the top section:

$$\boldsymbol{X} = \left[r_{d_1,T}, r_{d_2,T}, \ldots, r_{d_{Nd},T}, \frac{VT}{F}\right]^T \qquad (18)$$

(superscript T denotes transposed). The equation set (16) can then be written as a linear equation set in matrix form:

$$\mathbf{M}\cdot\mathbf{X} = \mathbf{Z} \qquad (19)$$

or

$$\begin{bmatrix} \frac{\alpha_{d_1} z_{d_1}}{\alpha_{d_1} - \theta_{d_1}} & \frac{\alpha_{d_2} z_{d_2}}{\alpha_{d_2} - \theta_{d_1}} & \cdots & \frac{\alpha_{d_{Nd}} z_{d_{Nd}}}{\alpha_{d_1} - \theta_{d_1}} & -1 \\ \frac{\alpha_{d_1} z_{d_1}}{\alpha_{d_1} - \theta_{d_2}} & \frac{\alpha_{d_2} z_{d_2}}{\alpha_{d_2} - \theta_{d_2}} & \cdots & \frac{\alpha_{d_{Nd}} z_{d_{Nd}}}{\alpha_{d_1} - \theta_{d_2}} & -1 \\ \cdots & \cdots & \cdots & \cdots & -1 \\ \frac{\alpha_{d_1} z_{d_1}}{\alpha_{d_1} - \theta_{d_{Nd-1}}} & \frac{\alpha_{d_2} z_{d_2}}{\alpha_{d_2} - \theta_{d_{Nd-1}}} & \cdots & \frac{\alpha_{d_{Nd}} z_{d_{Nd}}}{\alpha_{d_1} - \theta_{d_{Nd-1}}} & -1 \end{bmatrix}.$$

$$\begin{bmatrix} r_{d_1,T} \\ r_{d_2,T} \\ \cdots \\ r_{d_{Nd},T} \\ V_T/F \end{bmatrix} = \begin{bmatrix} -\sum_{i=1}^{d_1-1} \frac{\alpha_i z_i}{\alpha_i - \theta_{d_1}} \\ -\sum_{i=1}^{d_1-1} \frac{\alpha_i z_i}{\alpha_i - \theta_{d_2}} \\ \cdots \\ -\sum_{i=1}^{d_1-1} \frac{\alpha_i z_i}{\alpha_i - \theta_{d_{Nd-1}}} \end{bmatrix}$$

The elements in each column of $\mathbf{M}$ arise from the terms in (16) related to the distributing components, and we have one row for each active root. $\mathbf{Z}$ contains the part of (16) arising from the nondistributing light components with the recovery one in the top. The recoveries for the heavy nondistributing components are zero in the top, so these terms disappear.

There are $N_a = N_d - 1$ equations (rows of $\mathbf{M}$ and $\mathbf{Z}$) and $N_d + 1$ variables in $\mathbf{X}$ (columns in $\mathbf{M}$). Thus, by specifying any two of the variables in $\mathbf{X}$ as our degrees of freedom, we are left with $N_d - 1$ unknowns which can be solved from the linear equation set in (19).

To specify the product split, we introduce D/F as an extra variable in $\mathbf{X}$ and the following extra equation:

$$D/F = \sum r_{i,T} z_i \qquad (20)$$

Note that (19) is only valid in a certain region of the possible operating space, namely, in the region where components numbered d_1 to d_{N_d} are distributing to both products.

For nonsharp key specifications, components lighter than the light key, and heavier than the heavy key, may or may not be distributing. Then we usually have to check several possible distribution sets. See work by Halvorsen[14] for more details.

For $V > V_{\min}$ and an infinite number of stages, there are no common Underwood roots. Thus, at most one component may be distributing and its recovery is independent of the actual value of V, but it is uniquely

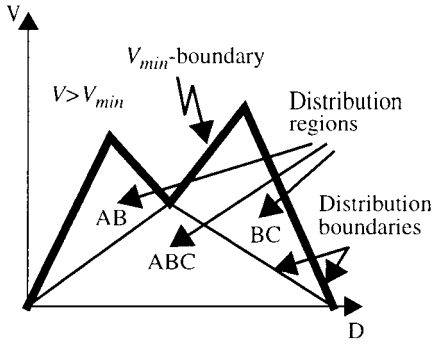

Figure 2. V_{min} diagram for a ternary feed (ABC).

related to D/F through (20):

$$D/F = z_1 + z_2 + ... + r_{d_1} z_{d_1} \tag{21}$$

4. V_{min} Diagram (Minimum-Energy Mountain)

A nice feature, because there are only 2 degrees of freedom, is that we can visualize the entire operating range in two dimensions, even with an arbitrary number of feed components. We choose to use (a) vapor flow per unit feed (V/F) and (b) product split, expressed by the distillate (D/F), as degrees of freedom (when we in some places use V and D, then we are implicitly assuming $F = 1$). The choice of vapor flow rate on the ordinate provides a direct visualization of the energy consumption and column load. We chose to use the vapor flow in the top (V_T) on the ordinate when the feed quality $q \neq 1$.

An important boundary is the transition from $V > V_{min}$ to $V = V_{min}$. It looks like mountain peaks in the $D-V$ plane, as illustrated in Figure 2, the V_{min} diagram.

There is a unique minimum-energy solution for each feasible pair of product recovery specifications, and the solution is always found below or at the V_{min} boundary.

Above the V_{min} boundary, the operation is not unique because we can always reduce the vapor rate down to the V_{min} boundary without changing the product specifications. Below the V_{min} boundary, we can identify a set of polygon regions for each set of distributing components. For the ternary case in Figure 7, the regions where AB, BC, or all of ABC are distributing are indicated. The boundaries between regions of distributing components are straight line segments in the $D-V$ plane due to the linear properties of (19) and (20).

Feasible operation requires positive vapor and liquid flows in all sections:

$$V_T > 0,\ V_B > 0,\ L_T > 0,\ L_B > 0 \tag{22}$$

In an ordinary two-product column, we must also require $D = V_T - L_T \geq 0$ and $B = L_B - V_B \geq 0$ (note that this is not a feasibility requirement for directly coupled sections), which with a single feed translates to (see Figure 3)

$$V_T \geq \max[(1-q)F, D] \quad \text{and} \quad 0 \leq D/F \leq 1 \tag{23}$$

The procedure for computing points to draw the V_{min} mountain diagram for a general multicomponent case (N_c components) is given in Table 2.

Because we assume constant relative volatility, only adjacent groups of components can be distributing.

In the V_{min} diagram, each peak represents minimum-energy operation for sharp splits between adjacent components ($r_{j,T} = 1$ and $r_{j+1,T} = 0$). Then there is only a single active Underwood root, and the minimum vapor flow and the corresponding distillate flow solved from (16) are simplified to

$$\text{Peaks:} \quad \frac{V_{T,\min}^{j/j+1}}{F} = \sum_{i=1}^{j} \frac{\alpha_i z_i}{\alpha_i - \theta_j} \quad \text{and} \quad \frac{D}{F} = \sum_{i=1}^{j} z_i \tag{24}$$

4.1. Binary Case. Before we explore the multicomponent cases, let us look closer at a binary case. Consider a feed with light component A and heavy component B with relative volatilities [α_A, α_B], feed composition $z = [z_A, z_B]$, feed flow rate $F = 1$, and liquid fraction q. In this case we obtain from the feed equation (14) a single common root θ_A obeying $\alpha_A > \theta_A > \alpha_B$. The minimum vapor flow is found by applying this root in the defining equation (16):

$$\frac{V_{T,\min}}{F} = \frac{\alpha_A r_{A,T} z_A}{\alpha_A - \theta_A} + \frac{\alpha_B r_{B,T} z_B}{\alpha_B - \theta_A} \tag{25}$$

We also have from (20)

$$\frac{D}{F} = r_{A,T} z_A + r_{B,T} z_B \tag{26}$$

The procedure in Table 2 becomes very simple in the binary case because there is only one possible pair of key components (A, B). We obtain the following results as illustrated in Figure 3. There is one sharp split (between A and B):

P_{AB}:

$$[r_{A,T}, r_{B,T}] = [1, 0] \rightarrow [D, V_{T,\min}] = \left[z_A, \frac{\alpha_A z_A}{\alpha_A - \theta_A}\right] F$$

The two asymptotic points are

P_0: $[r_{A,T}, r_{B,T}] = [0, 0] \rightarrow [D, V_{T,\min}] = [0, 0]$

P_1: $[r_{A,T}, r_{B,T}] = [1, 1] \rightarrow [D, V_{T,\min}] = [1, 1-q]F$

These three points make up a triangle as shown in Figure 3. Along the straight line P_0-P_{AB}, we have $V = V_{min}$ for a pure top product ($r_{B,T} = 0$), and from (25) the line can be expressed by the recovery $r_{A,T}$ or D/F:

$$\frac{V_T}{F} = \frac{\alpha_A r_{A,T} z_A}{\alpha_A - \theta_A} = \frac{\alpha_A \quad D}{\alpha_A - \theta_A F F} \text{ because } \frac{D}{F} = r_{A,T} z_A \tag{27}$$

Similarly, along the straight line $P_{AB}-P_1$, we have $V = V_{min}$ for a pure bottom product ($r_{A,T} = 1$), and the line can be expressed by the recovery $r_{B,T}$ or D/F:

$$\frac{V_T}{F} = \frac{\alpha_A z_A}{\alpha_A - \theta_A} + \frac{\alpha_B r_{B,T} z_B}{\alpha_B - \theta_A} \text{ where } \frac{D}{F} = z_A + r_{B,T} z_B \tag{28}$$

Inside the triangle, we may specify any pair of variables among (V_T, D, r_A, r_B) and use the equation set

Table 2. Computation Procedure for Construction of a V_{min} Diagram

1	find all possible common Underwood roots [θ_1, θ_2, ..., θ_{N_c-1}] from the feed equation (14)
2	use (19) and (20) to find the full solutions for a sharp split between every possible pair of light (LK) and heavy key (HK) specifications; each solution gives the component recoveries (R), minimum vapor flow (V_{min}/F), and product split (D/F); these are the peaks and knots in the diagram (P_{ij}), and there are $N_c(N_c-1)/2$ such key combinations:
	$N_c - 1$ cases with no intermediates (e.g., AB, BC, CD, ...); these points are the peaks in the V_{min} diagram
	$N_c - 2$ cases with one intermediate (e.g., AC, BD, CE, ...); these are the knots between the peaks, and the line segments between the peaks and these knots form the V_{min} boundary
	...
	two cases with $N_c - 3$ intermediates ($N_c - 1$ components distribute)
	one case with $N_c - 2$ intermediates (the preferred split)
3	find the two asymptotic points where all recoveries in the top are 0 or 1, respectively: $V_{T,min} = 0$ for $D = 0$ and $V_{T,min} = (1 - q)F$ for $D = F$

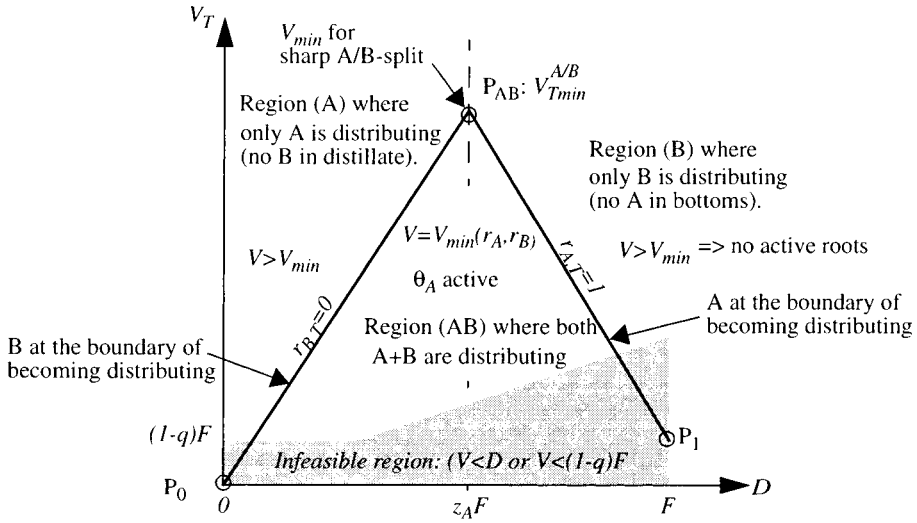

Figure 3. V_{min} diagram, or minimum-energy mountain, for binary separation between components A (light) and B (heavy). Visualization of the regions of distributing components.

of (25) and (26) to solve for the others. This is exactly the same equation set as given in (19) and (20) for the general multicomponent case when both components are distributing.

Above the triangle (V_{min} mountain), where $V > V_{min}$, we have no active Underwood roots, so (25) no longer applies. However, because only one component is distributing, we have either $r_{A,T} = 1$ or $r_{B,T} = 0$. This implies that the recoveries are directly related to D, and we have

$$\frac{D}{F} = r_{A,T}z_A \text{ for } \frac{D}{F} \le z_A \quad \text{or}$$

$$\frac{D}{F} = z_A + r_{B,T}z_B \text{ for } \frac{D}{F} \ge z_A \quad (29)$$

which is equivalent to (21) in the general multicomponent case. Anywhere above the triangle, we obviously waste energy because the same separation can be obtained by reducing the vapor flow until we hit the boundary to region AB.

$V_T > D$ and $V_T > (1-q)F$ are required for feasible operation of a conventional two-product distillation column. The shaded area represents an infeasible region where a flow rate somewhere in the column would be negative. Note that the asymptotic points (P_0 and P_1) are infeasible in this case.

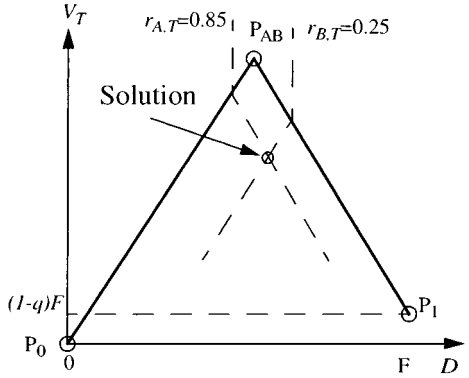

Figure 4. Solution for a given pair of recovery specifications visualized in the V_{min} diagram.

We may also visualize the nonsharp split solutions with specified component recoveries. This is illustrated in Figure 4 for the example $V_{T|r_A=0.85}(D)$ and $V_{T|r_B=0.25}(D)$ (dashed lines). Note that for $V > V_{min}$ these become vertical lines. The unique solution with both specifications fulfilled is at the intersection inside region AB denoted as "Solution" in Figure 4.

4.2. Ternary Case. Figure 5 shows an example of the V_{min} diagram, or minimum-energy mountain, for a ternary feed (ABC). To plot this diagram, we apply the procedure in Table 2 and identify the following five points:

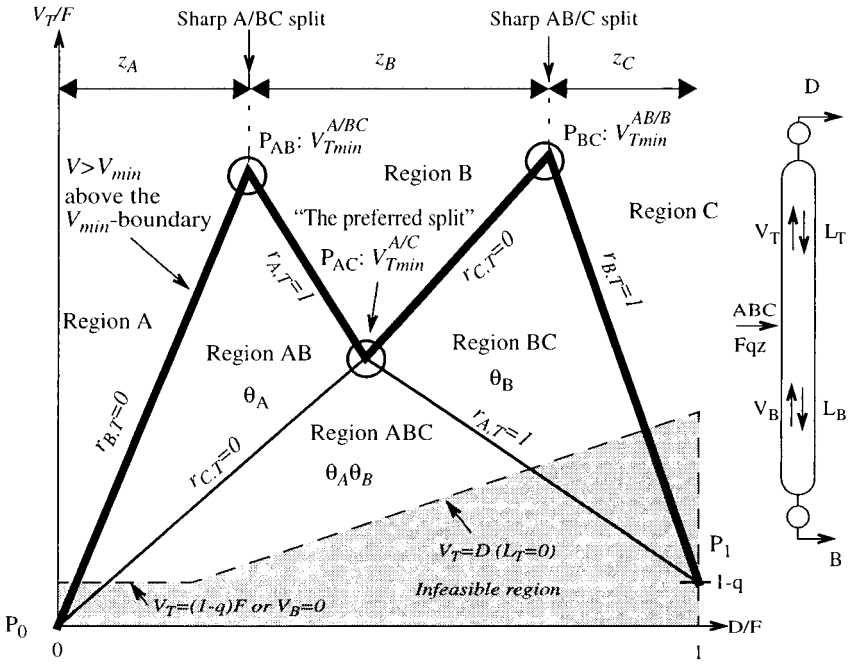

Figure 5. V_{min} diagram for a ternary feed mixture (ABC). $V > V_{min}$ above the V_{min} boundary (the "mountain" P_0−P_{AB}−P_{AC}−P_{BC}−P_1). All minimum-energy solutions, $[V = V_{min}(Spec_1,Spec_2)]$ are found in the distribution regions AB, BC, and ABC. The active Underwood roots are also indicated in each region (when $\phi_i = \theta_i$).

The peaks, which give V_{min} for sharp splits A/B and B/C (no distributing components):

P_{AB}:

$$[r_{A,T}, r_{B,T}] = [1, 0] \rightarrow [D, V_{T,min}] = \left[z_A, \frac{\alpha_A z_A}{\alpha_A - \theta_A}\right]F$$

P_{BC}: $[r_{B,T}, r_{C,T}] = [1, 0] \rightarrow [D, V_{T,min}] =$

$$\left[z_A + z_B, \frac{\alpha_A z_A}{\alpha_A - \theta_B} + \frac{\alpha_B z_B}{\alpha_B - \theta_B}\right]F$$

The preferred split, which gives V_{min} for sharp A/C split (B is distributing):

P_{AC}: $[r_{A,T}, r_{C,T}] = [1, 0] \rightarrow [D, V_{T,min}] =$

$$\left[z_A + \beta z_B, \frac{\alpha_A z_A}{\alpha_A - \theta_B} + \frac{\alpha_B z_B}{\alpha_B - \theta_B}\right]F$$

where β is the recovery of B: $\beta = r_{B,T}^{A/C} = -\alpha_A z_A(\alpha_B - \theta_A)(\alpha_B - \theta_B)/\alpha_B z_B(\alpha_A - \theta_A)(\alpha_A - \theta_B)$

The trivial asymptotic points:

P_0: $[r_{A,T}, r_{B,T}] = [0, 0] \rightarrow [D, V_{T,min}] = [0, 0]$

P_1: $[r_{A,T}, r_{B,T}] = [1, 1] \rightarrow [D, V_{T,min}] = [1, 1 - q]F$

The two peaks (P_{AB} and P_{BC}) give us the minimum vapor flow for sharp split between A/B and B/C, respectively. The valley, P_{AC}, gives us the minimum vapor flow for a sharp A/C split, and this occurs for a specific distribution of the intermediate component B, known as the "preferred split" (Stichlmair[19]).

One part of the V_{min} boundary, namely, the V-shaped P_{AB}−P_{AC}−P_{BC} curve, has been presented by several authors, e.g., Fidkowski[10] and Christiansen and Skogestad.[17] It gives the minimum vapor flow for a sharp split between A and C as a function of the distillate flow, or the distribution of the intermediate component (B). Figure 5, however, gives the complete diagram for all feasible operating points. In every region where more than one component may be distributing to both products (AB, BC, and ABC), at least one Underwood root is active, and we may find the actual flows and component distribution using (19). Note that at the boundaries one of the components is at the limit of being distributing:

At boundaries B/AB and ABC/BC: $r_{A,T} = 1$ ($r_{A,B} = 0$)

At boundary A/AB: $r_{B,T} = 0$ ($r_{B,B} = 1$)

At boundary C/CB: $r_{B,T} = 1$ ($r_{B,B} = 0$)

At boundaries B/BC and AB/ABC:

$r_{C,T} = 0$ (or $r_{C,B} = 1$)

4.3. Five-Component Example. A five-component example is shown in Figure 6. Here we also plot the contour lines for constant values of the recoveries in the top for each component in the range 0.1−0.9, and we clearly see how each component recovery depends on the operating point (D, V).

Note that the boundary lines (solid bold) are contour lines for top recoveries equal to 0 or 1 and that any contour line is vertical for $V > V_{min}$. The contour lines for different recovery values of a certain component are parallel in each region.

To draw the V_{min} diagram for N_c components, we must identify the $N_c(N_c - 1)/2$ points (P_{ij}) given in the procedure in Table 2, corresponding to the following distribution regions: AB, BC, CD, DE, ABC, BCD, CDE, ABCD, BCDE, ABCDE. Note that the behavior in a region where only two components are distributing is very similar to the simple binary case described in

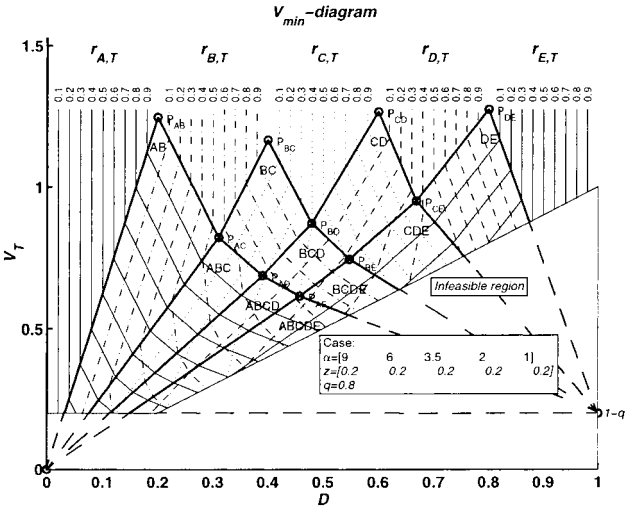

Figure 6. V_{min} diagram for a five-component feed ($F = 1$). Contour lines for constant top product recoveries are included.

section 4.1 and can be expressed by the single active common Underwood root in the actual region.

Figure 6 also illustrates that some combinations of recovery specifications can be infeasible, e.g. $r_{A,T} = 0.9$ and $r_{C,T} = 0.6$. Observe that a combined specification of D and an intermediate recovery may have multiple solutions, e.g., $D = 0.2$ and $r_{B,T} = 0.3$. The specification of V and a recovery will be unique, as will the specification of D and V. The specification of two (feasible) recoveries will also be unique, and the solution will always be a minimum-energy solution ($V = V_{min}$).

5. V_{min} Diagram by Rigorous Simulation

So far, we have used analytical expressions to compute the V_{min} diagram for ideal mixtures with constant molar flows and constant relative volatilities. However, for real mixtures we may replace the analytical Underwood equations with numerical property calculations and draw the V_{min} diagram. To approximate the vapor flow with an infinite number of stages, we should use *at least* $4N_{min}$ stages in the simulations, where N_{min} is the minimum number of stages for the separation (with infinite flows).

In the example described below, we applied the Hysys process simulator, using the Peng−Robinson equation of state, for an equimolar feed mixture of *n*-pentane (A), *n*-hexane (B), and *n*-heptane (C) at 745 kPa with 80% liquid fraction. The results are visualized in Figure 7, and the numerical values are listed in Table 3. The main diagram can be constructed by three simulations at the three characteristic points of the diagram (P_{AC}, P_{AB}, P_{BC}). In addition, we have also simulated some additional operating points to verify the internals of the diagram.

The V_{min} diagram for the real mixture (solid), drawn through the results of the rigorous simulations (circles), is very close to the ideal V_{min} diagram (dashed) computed with the assumption of constant relative volatilities ($\alpha = [1.683, 0.9266, 0.5234]$, which are the K values at the feed stage from simulation no. 3 in Table 3). The contour lines for constant recovery $r_{A,T} = 0.8$ and $r_{C,T} = 0.222$ for the constant relative volatility case are also shown (dotted). The match in region ABC is very good, as expected, because the pinch zone composition and thereby the relative volatilities will be con

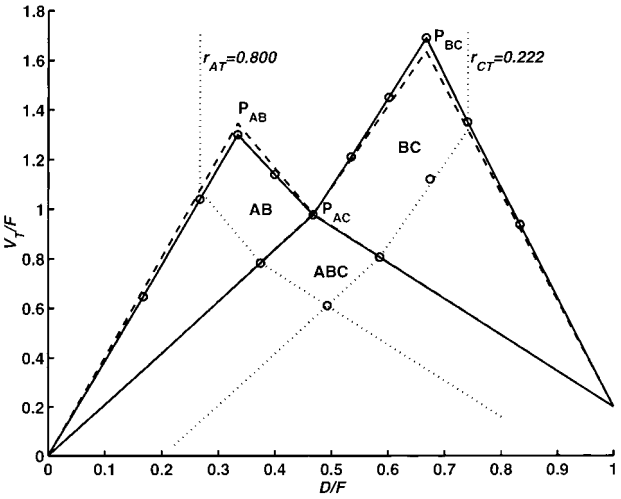

Figure 7. V_{min} diagram based on numerical simulations (solid) and constant relative volatilities (dashed). Each numerical simulation from Table 3 is indicated (circles). The contour lines for the selected constant (nonsharp) recoveries (dotted) are computed with constant relative volatilities. (Constant α values are from the simulation at P_{AC}).

Table 3. Rigorous Simulation Results for the Given Set of Specifications

	specification of 2 DOFs ($\epsilon = 0.001$)		simulation		constant α
			D	V_T	V_T
1: P_{AB}	$\boldsymbol{x_{B,T} = \epsilon}$	$\boldsymbol{x_{A,B} = \epsilon}$	**0.333**	**1.30**	**1.34**
2	$r_{B,T} = 0.2$	$x_{A,B} = \epsilon$	0.399	1.14	1.16
3: P_{AC}	$\boldsymbol{x_{C,T} = \epsilon}$	$\boldsymbol{x_{A,B} = \epsilon}$	**0.467**	**0.977**	**0.977**
4	$x_{C,T} = \epsilon$	$r_{B,T} = 0.6$	0.534	1.21	1.12
5	$x_{C,T} = \epsilon$	$r_{B,T} = 0.8$	0.601	1.45	1.42
6: P_{BC}	$\boldsymbol{x_{C,T} = \epsilon}$	$\boldsymbol{x_{B,B} = \epsilon}$	**0.667**	**1.69**	**1.63**
7	$r_{A,T} = 0.8$	$x_{B,T} = \epsilon$	0.267	1.04	1.08
8	$r_{A,T} = 0.8$	$x_{C,T} = \epsilon$	0.374	0.783	0.783
9	$r_{A,T} = 0.8$	$r_{C,T} = 0.222$	0.492	0.611	0.611
10	$x_{A,B} = \epsilon$	$r_{C,T} = 0.222$	0.585	0.806	0.806
11	$r_{B,T} = 0.8$	$r_{C,T} = 0.222$	0.674	1.12	1.10
12	$x_{B,B} = \epsilon$	$r_{C,T} = 0.222$	0.740	1.35	1.32
13	$r_{A,T} = 0.5$	$x_{B,T} = \epsilon$	0.167	0.647	0.672
14	$x_{C,T} = 0.2$	$x_{B,B} = \epsilon$	0.833	0.937	0.917

stant for the real mixture too. Further away from region ABC we observe a certain deviation between the real and ideal diagrams. The explanation is that the pinch zone composition at the feed stage will change a little outside region ABC and so will the real relative volatility.

However, we conclude that the V_{min} diagram can be applied for assessment of real mixtures too. Obviously there can be some nonlinearities of the distribution boundaries and some deviations in the height of the peaks for the real mixture because the relative volatilities and molar flows are not constants, but the main picture is very similar.

Note that the vapor flow is the amount leaving the feed stage. To get an exact prediction of the reboiler and condenser flows, we have to take into account the difference in heat of vaporization for the mixture at the feed stage and in the respective column ends. We also expect that the pinch zone compositions in each of the column ends will be slightly different from those of the ideal case because the relative volatilities and molar flows will not be completely constant along the column.

In the example Fenske's minimum reflux formula gives $4N_{min} \approx 4 \log \epsilon^{-2}/\log \min(\alpha_{ij}) \approx 100$, which is the stage number used in the simulations. Note that with

a finite number of stages we reach an approximate distribution boundary by specifying a small composition (here $\epsilon = 0.001$) of the component to be removed in the appropriate product instead of zero recovery. In practice, $N = 4N_{min}$ can be regarded as close to the infinite number of stages in a simulation.

6. Discussion

In the thesis by Halvorsen,[14] some points on the usage of the V_{min} diagram and further analysis are discussed in more detail. Here we only summarize a few of these results.

1. Behavior of all of the Underwood roots as a function of the operating point (pp 83 and 84). The V_{min} diagram is also very well suited to illustrate the behavior of the Underwood roots in each section (ϕ, ψ) as we change the operating conditions. Recall that Underwood showed that, as the vapor flow (V) is reduced, a certain pair of roots will coincide, and we get $V = V_{min}$. However, how do we find which pair and what happens to the other roots?

2. Relation to composition profiles and pinch zones (pp 85−90, 101, and 102). It can be shown for the ternary case that the pinch zone composition (subscript P) when one component is removed completely somewhere in one of the column ends depends only on the actual Underwood root between the volatilities of the remaining components. In the top we obtain[14]

$$x_{A,PT} = \frac{\alpha_B(\alpha_A - \phi_A)}{\phi_A(\alpha_A - \alpha_B)}, \quad x_{B,PT} = 1 - x_{A,PT} \qquad (30)$$

Thus, in the minimum-energy regions (AB and ABC) where $\phi_A = \theta_A$ this result tells that the pinch zone composition above the feed stage is constant. This is extremely interesting when we consider the Petlyuk arrangement because the feed stage of the succeeding column is "connected" to this pinch zone.

3. Finite number of stages (pp 42−48, 90−92, and 126−129). It is straightforward to determine the minimum number of stages in a section from the product purity specifications with Fenske's formula. The largest number of real stages in order to carry out a sharp split between the two most extreme components is required close to the preferred split. Away from the preferred split, the number of required stages in one of the sections above or below the feed stage is reduced. Thus, if the column is designed for operation on one side of the preferred split, this can be taken advantage of by reducing the number of stages in the appropriate section. However, if the column is to be operated at or on both sides of the preferred split, both sections have to be designed with its maximum required number of stages.

7. Conclusion

The distribution of feed components and corresponding minimum energy requirement is easily found by just a glance at the V_{min} diagram. The characteristic peaks and knots are easily computed from Underwood's equations for an infinite number of stages. The heights of the peaks, and thereby the energy requirement for sharp splits, are determined by the relative volatilities and the feed composition. The highest peak characterizes the most difficult binary split.

The V_{min} diagram can be computed for nonideal systems too, e.g., by using a commercial rigorous simulator with a large number of stages. Thus, this graphical tool is not limited to the ideal system assumptions.

However, for ideal systems, we provide exact analytical expressions for minimum-energy calculations for the entire feasible operating range of a distillation column.

Although the theory has been deduced for a single conventional column, the simple V_{min} diagram for a two-product column contains all of the information needed for optimal operation of a complex directly (fully thermally) coupled arrangement, such as the Petlyuk column. This is the subject of parts 2 and 3 of this series.

Literature Cited

(1) Underwood, A. J. V.; et al. Fractional Distillation of Ternary Mixtures. Part I. *J. Inst. Pet.* **1945**, *31*, 111−118.

(2) Underwood, A. J. V.; et al. Fractional Distillation of Ternary Mixtures. Part II. *J. Inst. Pet.* **1946**, *32*, 598−613.

(3) Underwood, A. J. V. Fractional Distillation of Multi-Component Mixtures—Calculation of Minimum Reflux Ratio. *J. Inst. Pet.* **1946**, *32*, 614−626.

(4) Underwood, A. J. V. Fractional Distillation of Multi-Component Mixtures. *Chem. Eng. Prog.* **1948**, *44* (No. 8).

(5) Shiras, R. N.; Hansson, D. N.; Gibson, C. H. Calculation of Minimum Reflux in Distillation Columns. *Ind. Eng. Chem.* **1950**, *42* (No. 18), 871−876.

(6) King, C. J. Separation Processes. *Chemical Engineering Series*; McGraw-Hill: New York, 1980.

(7) Franklin, N. L.; Forsyth, J. S. The interpretation of Minimum Reflux Conditions in Multi-Component Distillation. *Trans. Inst. Chem. Eng.* **1953**, *31* (reprinted in the Jubilee Supplement of *Trans. Inst. Chem. Eng.* **1997**, *75*).

(8) Wachter, J. A.; Ko, T. K. T.; Andres, R. P. Minimum Reflux Behaviour of Complex Distillation Columns. *AIChE J.* **1988**, *34* (No. 7), 1164−84.

(9) Koehler, J.; Poellmann, P.; Blass, E. A Review on Minimum Energy Calculations for Ideal and Nonideal Distillations. *Ind. Eng. Chem. Res.* **1995**, *34* (No. 4), 1003−1020.

(10) Fidkowski, Z.; Krolikowski, L. Thermally Coupled System of Distillation Columns: Optimization Procedure. *AIChE J.* **1986**, *32* (No. 4).

(11) Carlberg, N. A.; Westerberg, A. W. Temperature−Heat Diagrams for Complex Columns. 3. Underwood's Method for the Petlyuk Configuration. *Ind. Eng. Chem. Res.* **1989**, *28*, 1386−1397.

(12) Carlberg, N. A.; Westerberg, A. W. Temperature−Heat Diagrams for Complex Columns. 2. Underwood's Method for Side-strippers and Enrichers. *Ind. Eng. Chem. Res.* **1989**, *28*, 1379−1386.

(13) Neri, B.; Mazzotti, M.; Storti, G.; Morbidelli, M. Multicomponent Distillation Design Through Equilibrium Theory. *Ind. Eng. Chem. Res.* **1998**, *37*, 2250−2270.

(14) Halvorsen, I. J. Minimum Energy Requirements in Complex Distillation Arrangements. Dr. ing. Thesis, Norwegian University of Science and Technology (NTNU), Trondheim, Norway, 2001. Available from the web page of Sigurd Skogestad, Department of Chemical Engineering, NTNU (May 2002: http://www.chemeng.ntnu.no/~skoge/publications/thesis/2001/halvorsen/).

(15) Halvorsen, I. J.; Skogestad, S. Minimum Energy Consumption in Multicomponent Distillation. 2. Three-Product Petlyuk Arrangements. *Ind. Eng. Chem. Res.* **2003**, *42*, 605−615.

(16) Halvorsen, I. J.; Skogestad, S. Minimum Energy Consumption in Multicomponent Distillation. 3. More than Three Products and Generalized Petlyuk Arrangements. *Ind. Eng. Chem. Res.* **2003**, *42*, 616−629.

(17) Christiansen, A. C.; Skogestad, S. Energy Savings in Integrated Petlyuk Distillation Arrangements. Importance of Using the Preferred Separation. AIChE Annual Meeting, Los Angeles, Nov 1997; Paper 199d (updated version as found in work by Christiansen[18]).

(18) Christiansen, A. C. Studies on optimal design and operation of integrated distillation arrangements. Ph.D. Thesis, Norwegian University of Science and Technology (NTNU), Trondheim, Norway, 1997 http://www.chemeng.ntnu.no/~skoge/publications/thesis/2001/halvorsen/).

(19) Stichlmair, J. Distillation and Rectification. *Ullmann's Encyclopedia of Industrial Chemistry*; VCH: Weinheim, Germany, 1988; Vol. B3, pp 4-1−4-94.

Received for review October 19, 2001
Revised manuscript received June 3, 2002
Accepted June 24, 2002

IE010863G